Proceedings of the Korean Nuclear Society Autumn Meeting
Taejon, Korea, October 2000

The Calculation of Thermal Neutron Scattering Cross Sections for Bismuth Crystal

Young-Sik Cho, Choong-Sup Gil and Jonghwa Chang

Korea Atomic Energy Research Institute
150 Dukjin-dong, Yusong-gu, Taejon 305-353, Korea
yscho@kaeri.re.kr

Abstract

The module LEAPR of the NJOY data processing system has been improved to have the capability of computing the thermal elastic scattering cross sections for bismuth, which has a rhombohedral structure containing two atoms. The calculation formulas for thermal neutron elastic scattering by bismuth were introduced and incorporated into LEAPR, and then the scattering cross sections for bismuth were computed. The results were compared with the experimental data, and they were found to give a good agreement with the experimental data.

1. Introduction

At thermal energies the energy transferred by the scattering of a neutron is similar to the kinetic energy of atoms in liquids and solids, and the de Broglie wavelength is comparable to the interatomic distances. Hence, the characteristic motion of atoms and their structures should be taken into account to exactly describe the thermal scattering.

Polycrystalline bismuth is often used as a neutron filter expecially for generation of cold neutrons. It is required to determine the characteristics of thermal neutron scattering by bismuth to understand the properties of bismuth as a filter.

NJOY [1] is widely used as a nuclear data processing tool, and has a built-in module named LEAPR which is able to calculate thermal scattering cross sections for materials of hcp (hexagonal close packed) lattices such as beryllium. This module can also be used to calculate the thermal inelastic scattering cross sections for bismuth with only user defined data for the phonon frequency spectrum. However, the code cannot exactly compute thermal elastic

scattering cross sections for bismuth because the module does not take into account the structure of the bismuth lattice on which elastic scattering sensitively depends.

In the present article, the module LEAPR of NJOY is improved to have the capability of computing the thermal elastic scattering cross sections for bismuth polycrystal, which has a rhombohedral structure. The results are compared with experimental data, and they are found to give good agreement with experimental data.

2. Structure of Bismuth Lattice

Bismuth crystallizes in a rhombohedral structure with two atoms per unit cell. The rhombohedral angle is 57.23 ^{o} and the atomic positional parameter z is 0.23389 at 298 ^{o}K [2].

In the case of a rhombohedral lattice, primitive lattice vector $\boldsymbol{T}$ can be expressed as:

$$\boldsymbol{T} = u_1\boldsymbol{a}_1 + u_2\boldsymbol{a}_2 + u_3\boldsymbol{a}_3, \tag{1}$$

where u_1, u_2 and u_3 are integers which can take all possible values including zero, and $\boldsymbol{a}_1, \boldsymbol{a}_2$ and $\boldsymbol{a}_3$ are the primitive translation vectors which construct the primitive unit cell, defined as:

$$\begin{aligned}
\boldsymbol{a}_1 &= \frac{1}{2}a_H\hat{\boldsymbol{x}} - \frac{1}{2\sqrt{3}}a_H\hat{\boldsymbol{y}} + \frac{1}{3}c_H\hat{\boldsymbol{z}} \\
\boldsymbol{a}_2 &= \frac{1}{\sqrt{3}}a_H\hat{\boldsymbol{y}} + \frac{1}{3}c_H\hat{\boldsymbol{z}} \\
\boldsymbol{a}_3 &= -\frac{1}{2}a_H\hat{\boldsymbol{x}} - \frac{1}{2\sqrt{3}}a_H\hat{\boldsymbol{y}} + \frac{1}{3}c_H\hat{\boldsymbol{z}}
\end{aligned} \tag{2}$$

where $\hat{\boldsymbol{x}}, \hat{\boldsymbol{y}}$ and $\hat{\boldsymbol{z}}$ are the unit vectors in a cartesian coordinate system, and a_H and c_H are lattice constants referred to the hexagonal coordinate system. For bismuth, the lattice constant a_H is 4.546 Å and c_H is 11.863 Å [2].

The reciprocal lattice vector is defined as

$$\boldsymbol{\tau} = l_1\boldsymbol{b}_1 + l_2\boldsymbol{b}_2 + l_3\boldsymbol{b}_3 \ , \tag{3}$$

where l_1, l_2 and l_3 are integers which can take all possible values including zero, and

$\boldsymbol{b}_1$, $\boldsymbol{b}_2$ and $\boldsymbol{b}_3$ are primitive translation vectors of a reciprocal lattice, defined as:

$$\begin{aligned}
\boldsymbol{b}_1 &= 2\pi \frac{\boldsymbol{a}_2 \times \boldsymbol{a}_3}{\boldsymbol{a}_1 \cdot \boldsymbol{a}_2 \times \boldsymbol{a}_3} = 2\pi \left[\frac{1}{a_H} \hat{\boldsymbol{x}} - \frac{1}{\sqrt{3} a_H} \hat{\boldsymbol{y}} + \frac{1}{c_H} \hat{\boldsymbol{z}} \right] \\
\boldsymbol{b}_2 &= 2\pi \frac{\boldsymbol{a}_3 \times \boldsymbol{a}_1}{\boldsymbol{a}_1 \cdot \boldsymbol{a}_2 \times \boldsymbol{a}_3} = 2\pi \left[\frac{2}{\sqrt{3} a_H} \hat{\boldsymbol{y}} + \frac{1}{c_H} \hat{\boldsymbol{z}} \right] \\
\boldsymbol{b}_3 &= 2\pi \frac{\boldsymbol{a}_1 \times \boldsymbol{a}_2}{\boldsymbol{a}_1 \cdot \boldsymbol{a}_2 \times \boldsymbol{a}_3} = 2\pi \left[-\frac{1}{a_H} \hat{\boldsymbol{x}} - \frac{1}{\sqrt{3} a_H} \hat{\boldsymbol{y}} + \frac{1}{c_H} \hat{\boldsymbol{z}} \right]
\end{aligned} \tag{4}$$

and it is evident from (2) and (4) that

$$\boldsymbol{a}_i \cdot \boldsymbol{b}_j = 2\pi \delta_{ij} , \tag{5}$$

where the symbol δ_{ij} is the Kronecker delta.

3. Elastic Scattering

Through the thermal elastic scattering by the bound nuclei, the energy of a neutron remains unchanged. This should be distinguished from the elastic scattering by a single particle where the neutron loses energy. The thermal elastic scattering can be divided into two parts: coherent scattering and incoherent scattering. For crystalline solids such as bismuth, scattered waves interfere with each other, resulting in so-called Bragg scattering, which is coherent elastic scattering. The incoherent effect is important for hydrogenous materials and neglected in this work.

3.1 Bragg Scattering

As a consequence of symmetry of the crystal lattice, Bragg scattering occurs if

$$\Delta \mathbf{k} = \mathbf{k} - \mathbf{k}' = \boldsymbol{\tau}(l_1, l_2, l_3), \tag{6}$$

where $\Delta \mathbf{k}$ is a scattering vector, $\mathbf{k}$ is the wave vector of the incident neutron, and $\mathbf{k}'$ is the wave vector of the scattered neutron.

Since the Bragg scattering is elastic ($|\mathbf{k}| = |\mathbf{k}'|$), it follows from (6) that

$$|\Delta \mathbf{k}| = 2k\sin\theta = |\boldsymbol{\tau}| = \frac{2\pi n}{d} \tag{7a}$$

or

$$2d\sin\theta = n\lambda \ , \tag{7b}$$

where θ is the Bragg angle between $\mathbf{k}$ and the Bragg planes which are orthogonal to $\boldsymbol{\tau}$. d is the spacing between Bragg planes, and λ is the wavelength of the incident neutron.

Eq. (7b) shows that no Bragg scattering can occur when the wavelength of the incident neutron is larger than twice the largest spacing d_{max} of Bragg planes. When λ reaches $2d_{max}$ ($k=\tau_{min}/2$, where τ_{min} is the smallest length of the reciprocal lattice vector), the first Bragg scattering occurs at the incident angle of 90^{o}. In crystalline solids, there exist many Bragg planes which satisfy Eq. (7b) and the energies corresponding to these critical values ($k_i=\tau_i/2$),

$$E_i = \frac{\hbar^2 k_i^2}{2m} = \frac{\hbar^2 \tau_i^2}{8m} \tag{8}$$

are usually called the Bragg edges. Here m is the mass of a neutron.

3.2 Elastic Cross Section for Bismuth

The coherent elastic cross section for a polycrystal [3] is given by

$$\sigma_{coh} = \frac{n\pi^2\sigma_c}{Vk^2} \sum_{\tau}^{\tau<2k} \frac{1}{\tau} e^{-2W(\tau)} |F(\boldsymbol{\tau})|^2 \ , \tag{9}$$

where n is the number of atoms in the primitive unit cell, V is the volume of the primitive unit cell, σ_c is the effective bound coherent scattering cross section for the material, $e^{-2W(\tau)}$ is the Debye-Waller factor, and $F(\boldsymbol{\tau})$ is the unit cell structure factor. The summation extends over all reciprocal lattice vectors whose magnitudes are not greater than 2k.

At each Bragg edge which satisfies Eq. (8), the coherent scattering cross section shows a sharp Bragg peak, and then decreases proportionally to E^{-1} with increasing neutron energy up to the next Bragg edge. Each Bragg peak arises by the reflection of neutrons from a new set of Bragg planes which satisfy Eq. (7b). At energies greater than 0.1 eV, the cross section varies smoothly due to the contribution of so many such planes.

The Debye-Waller factor reflects the influence of atomic motion on coherent elastic scattering. As the temperature of the material increases, the Debye-Waller factor decreases due to the increased thermal motion of the atoms, reducing the intensity of Bragg scattering. $W(\boldsymbol{\tau})$ in the Debye-Waller factor is calculated using the phonon frequency spectrum of the bismuth lattice in the module LEAPR. Fig. 1 shows the phonon frequency spectrum used for this work, which is expressed as a function of the phonon energy. This spectrum was taken from the results experimentally determined by Kress. [4]

The unit cell structure factor is defined as

$$F(\boldsymbol{\tau}) = \sum_{s=1}^{n} e^{i\boldsymbol{\tau}\cdot\boldsymbol{\rho}_s}, \tag{10}$$

where n is the number of atoms in the primitive unit cell and $\boldsymbol{\rho}_s$ is the positions of atoms in the primitive unit cell. If the crystalline structure is such that only one atom is contained per primitive unit cell, the structure factor is equal to 1. In the case of bismuth, there are two atoms in the primitive unit cell at positions (z,z,z), (-z,-z,-z), so that

$$\boldsymbol{\rho}_0 = z(\boldsymbol{a}_1 + \boldsymbol{a}_2 + \boldsymbol{a}_3), \quad \boldsymbol{\rho}_1 = -z(\boldsymbol{a}_1 + \boldsymbol{a}_2 + \boldsymbol{a}_3) \tag{11}$$

where z is the atomic positional parameter of bismuth.
Thus, using Eq. (3) and Eq. (5), we obtain

$$\begin{aligned} |F(\boldsymbol{\tau})|^2 &= |\sum_{s=1}^{n} e^{i\boldsymbol{\tau}\cdot\boldsymbol{\rho}_s}|^2 \\ &= |e^{i2\pi z(l_1+l_2+l_3)} + e^{-i2\pi z(l_1+l_2+l_3)}|^2 \\ &= 4\cos^2[2\pi z(l_1+l_2+l_3)] \end{aligned} \tag{12}$$

For a rhombohedral lattice, the volume of the primitive unit cell is

$$V = \boldsymbol{a}_1 \cdot \boldsymbol{a}_2 \times \boldsymbol{a}_3 = \frac{a_H^2 c_H}{2\sqrt{3}} \tag{13}$$

and, from Eq. (3) and Eq. (4), τ is given by

$$\tau = 2\pi\sqrt{\frac{1}{a_H^2}(l_1-l_3)^2+\frac{1}{3a_H^2}(-l_1+2l_2-l_3)^2+\frac{1}{c_H^2}(l_1+l_2+l_3)^2}$$
$$= 2\pi\sqrt{\frac{4}{3a_H^2}(l_1^2+l_2^2+l_3^2-l_1l_2-l_1l_3-l_2l_3)+\frac{1}{c_H^2}(l_1^2+l_2^2+l_3^2+2l_1l_2+2l_1l_3+2l_2l_3)} \quad (14)$$

4. Inelastic Scattering for Bismuth

Inelastic scattering includes both the coherent and incoherent contributions. The numerical calculation of such scattering is considerably simplified by two approximations: the incoherent approximation and the Gaussian approximation. In the incoherent approximation, the interference effect of inelastic scattering is neglected. The approximation is valid for neutrons with energies greater than about 0.001 eV where the interference effect is practically negligible. In the Gaussian approximation, the intermediate scattering function is represented as a Gaussian function of the scattering vector. The intermediate scattering function is such a function that describes the thermal scattering.

With these approximations, the inelastic scattering cross sections for thermal neutrons can be obtained from the exact shape of the phonon frequency distribution. The module LEAPR needs the phonon frequency spectrum of the material being considered as an input. We used the experimentally determined phonon frequency spectrum of bismuth [4].

5. Calculations and the Results

The formulas for the thermal neutron elastic scattering by bismuth, which were introduced in section 3.2, are incorporated into the module LEAPR of NJOY. The module is used to calculate the thermal elastic scattering cross sections for bismuth polycrystal. This method can also be applied for other materials which have rhombohedral structures such as arsenic and antimony. The effect of inelastic scattering is taken into account by using the phonon frequency spectrum of bismuth crystal. The calculations were performed at 77 ^{o}K and 298 ^{o}K. The physical constants used for the calculations are shown in Table 1.

The computed coherent elastic scattering cross sections showing the Bragg edges and peaks are graphed in Fig. 2. Notice that the cross section is zero for energies below 1.31 meV, which is called the Bragg cut-off. Each Bragg edge corresponds to the value obtained from Eq. (8). The Bragg peaks represent a positive interference of neutron waves scattered from a new set of Bragg planes in the bismuth lattice. The peaks are a little lower at higher temperatures because of the increased thermal motion of bismuth atoms.

In Figs. 3 and 4, inelastic cross sections and total scattering cross sections are shown. Notice that the computed inelastic cross sections are larger at higher temperatures due to the increased thermal motion of atoms.

In Fig. 5, the total cross sections computed at 298 ^{o}K are compared with the experimental data. The experimental data were given as the total cross sections, so for comparison, the theoretical total cross sections were obtained by adding the bismuth capture cross sections from ENDF/B-VI [5] to the total scattering cross sections calculated in this work. The experimental data were obtained from BNL-325 [6], and these experiments were performed at room temperature. It is evident from the figure that the calculated total cross sections give a good agreement with the measured data. The agreement for the Bragg edges is very good.

In Fig. 6, the scattering cross sections calculated at 298 ^{o}K are compared with the elastic cross section data from ENDF/B-VI. The cross section data from ENDF/B-VI are those for a single free nucleus. The elastic cross sections obtained from ENDF/B-VI are larger than the calculated values at lower energies but tend to coincide with them at higher energies.

6. Conclusions

An attempt to calculate the thermal neutron scattering cross sections for bismuth crystal was made in this article. The calculation formulas for thermal neutron elastic scattering cross sections for bismuth were introduced and incorporated into the module LEAPR of NJOY, and the scattering cross sections were then computed. The inelastic scattering cross sections were calculated using the experimentally determined phonon frequency spectrum for bismuth. This improved module can also be used to obtain the scattering cross sections for the other materials which have rhombohedral structures such as arsenic and antimony by changing the lattice constants and the coherent bound scattering cross section in the source code.

The calculated results were compared with the experimental data. The results were found to give a good agreement with the experimental data. Bragg edges and peaks shown in the calculated coherent elastic cross sections agreed well with those in the experimental data.

References

1. R. E. MacFarlane and D. W. Muir, "The NJOY Data Processing System Version 91," LA-12740-M (Oct. 1994).
2. P. Cucka and C. S. Barrett, "The Crystal Structure of Bi and of Solid Solutions of Pb, Sn, Sb and Te in Bi," Acta Cryst., **15**, 865 (1962).

3. D. E. Parks, M. S. Nelkin, J. R. Beyster, and N. F. Wikner, Slow Neutron Scattering and Thermalization, W. A. Benjamin, Inc., New York (1970).
4. W. Kress, "Phonon Dispersion Curves, One-Phonon Densities of States and Impurity Vibrations of Metallic Systems," Physik Daten, No. 26-1. Fachinformationszentrum, Karlsruhe (1987)
5. P. F. Rose, "Cross Section Evaluation Working Group, ENDF-VI Summary Documentation," BNL-NCS-17541 (ENDF-201) (1991).
6. D. I. Garber and R. R. Kinsey, BNL-325, 3rd ed. (1976).
7. S. F. Mughabghab, M. Divadeenam, N. E. Holden, Neutron Cross Sections: Vol. 1, Academic Press, New York (1981).

Table 1. The physical constants used for the calculations

Weight ratio to neutron	207.185
Lattice Constants; a_H, c_H	4.546 Å, 11.863 Å [2]
Rhombohedral Angle	57.23° [2]
Atomic Positional Parameter	0.23389 [2]
Coherent bound scattering cross section	9.134 barns [7]
Free atom scattering cross section	9.30 barns [7]

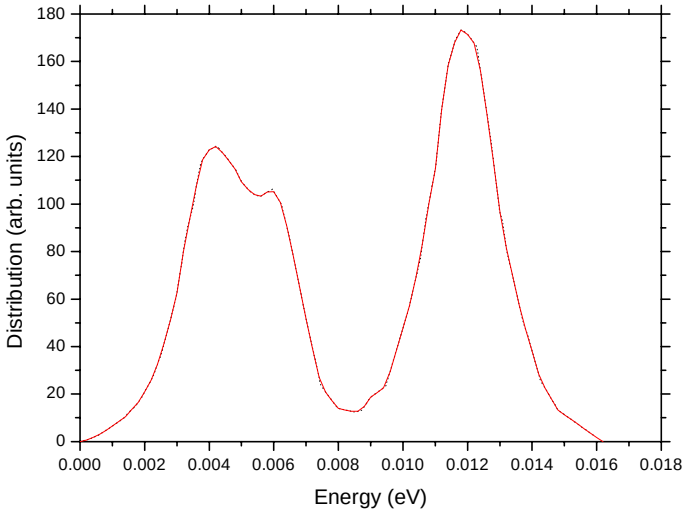

Fig. 1. The phonon frequency spectrum of Bi

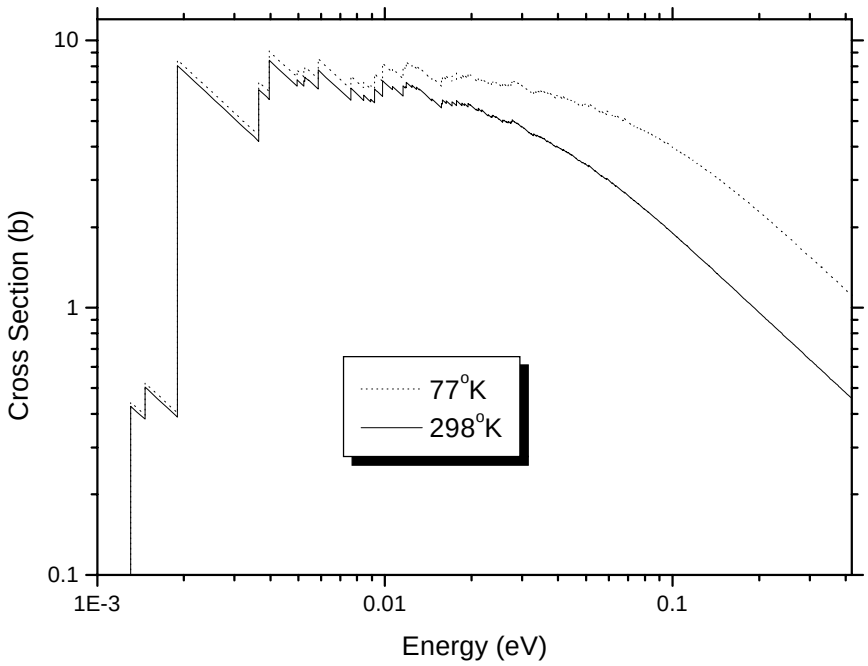

Fig. 2. The elastic cross sections for Bi

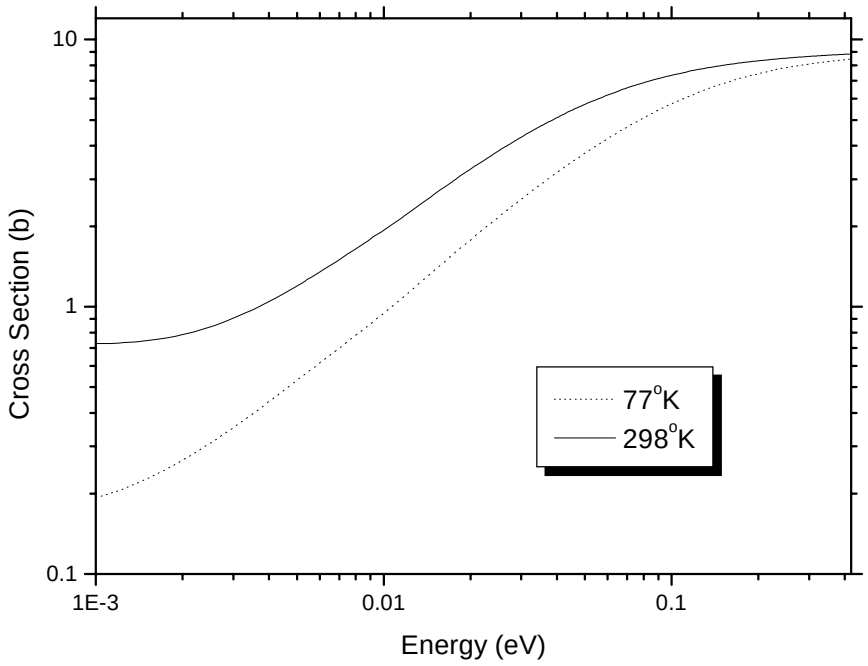

Fig. 3. The inelastic cross sections for Bi

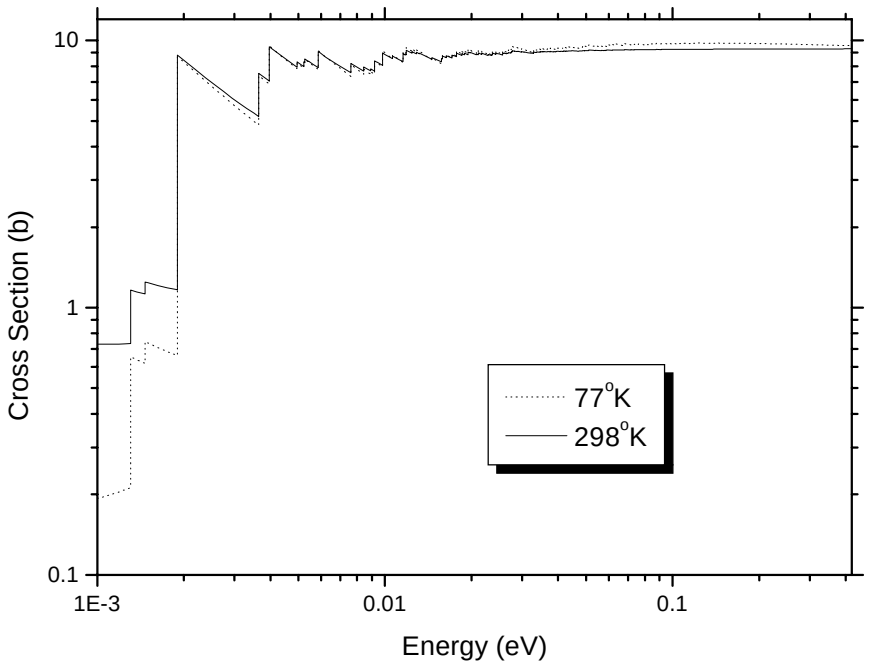

Fig. 4. The total scattering cross sections for Bi

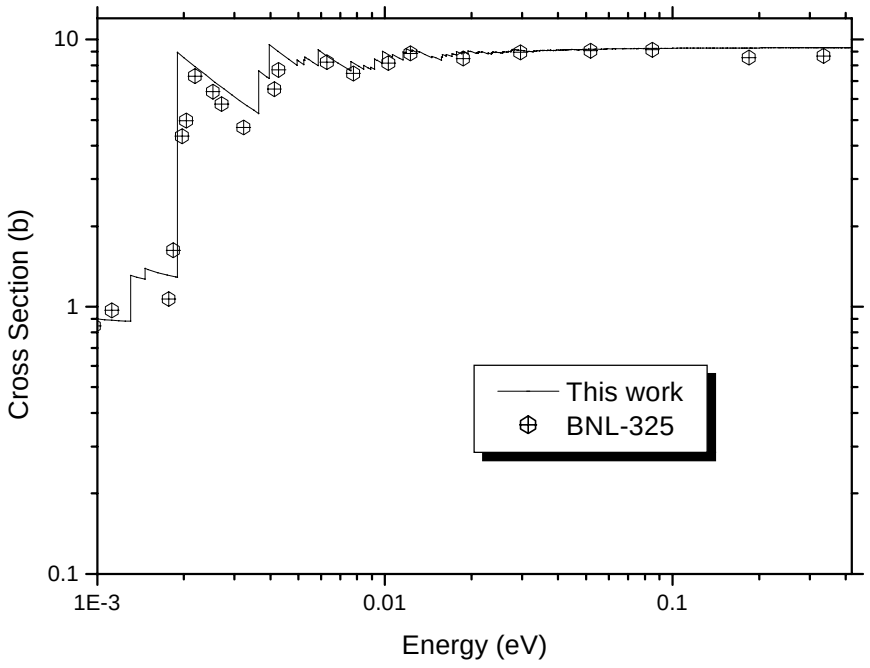

Fig. 5. The total cross sections at 298 °K for Bi

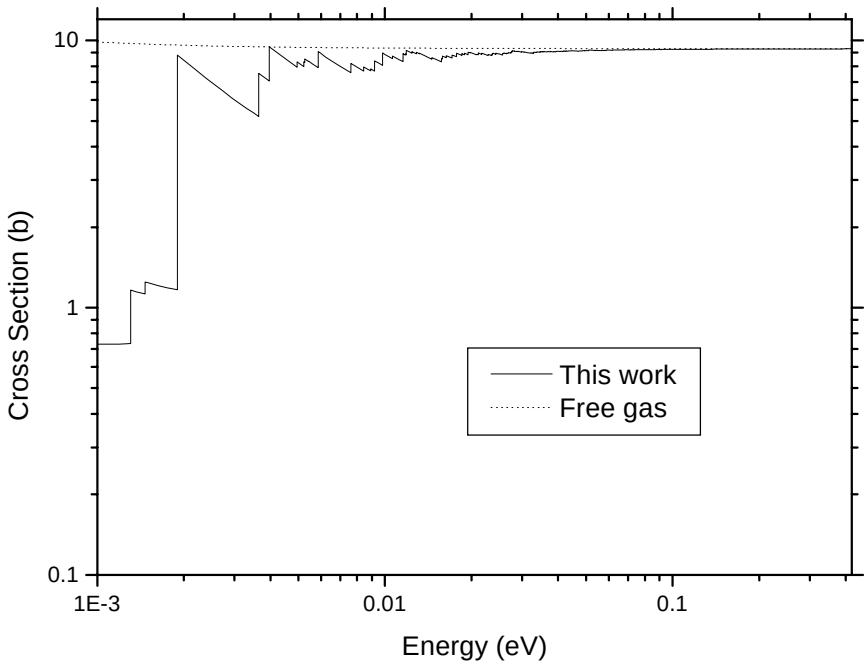

Fig. 6. The total scattering cross sections at 298 ^{o}K for Bi